

# Direction Matters: Monovalent Streptavidin/Biotin Complex under Load

Steffen M. Sedlak,<sup>1,†,‡</sup> Leonard C. Schendel,<sup>1,†,‡</sup> Marcelo C. R. Melo,<sup>‡,§,‡</sup> Diana A. Pippig,<sup>†</sup>  
Zaida Luthey-Schulten,<sup>‡,§,||</sup> Hermann E. Gaub,<sup>†,‡</sup> and Rafael C. Bernardi<sup>‡,‡,‡</sup>

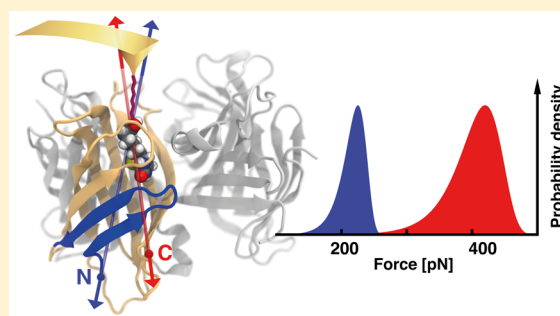
<sup>†</sup>Lehrstuhl für Angewandte Physik and Center for NanoScience (CeNS), Ludwig-Maximilians-Universität München, Amalienstrasse 54, 80799 Munich, Germany

<sup>‡</sup>Beckman Institute for Advanced Science and Technology, <sup>§</sup>Center for Biophysics and Quantitative Biology, and <sup>||</sup>Department of Chemistry, University of Illinois at Urbana–Champaign, Urbana, Illinois 61801, United States

## Supporting Information

**ABSTRACT:** Novel site-specific attachment strategies combined with improvements of computational resources enable new insights into the mechanics of the monovalent biotin/streptavidin complex under load and forced us to rethink the diversity of rupture forces reported in the literature. We discovered that the mechanical stability of this complex depends strongly on the geometry in which force is applied. By atomic force microscopy-based single molecule force spectroscopy we found unbinding of biotin to occur beyond 400 pN at force loading rates of 10 nN/s when monovalent streptavidin was tethered at its C-terminus. This value is about twice as high than that for N-terminal attachment. Steered molecular dynamics simulations provided a detailed picture of the mechanics of the unbinding process in the corresponding force loading geometries. Using machine learning techniques, we connected findings from hundreds of simulations to the experimental results, identifying different force propagation pathways. Interestingly, we observed that depending on force loading geometry, partial unfolding of N-terminal region of monovalent streptavidin occurs before biotin is released from the binding pocket.

**KEYWORDS:** Streptavidin/biotin, single-molecule force spectroscopy, atomic force microscopy, molecular dynamics, machine learning



The interaction of the small molecule biotin with the protein streptavidin (SA) is widely used for noncovalent, yet stable bonding in nanotechnology, biotechnology, and medicine.<sup>1</sup> The robustness of SA and the SA/biotin complex over a wide range of conditions, the comparatively easy fusion of biotin to nucleic acids, proteins, dyes, other macromolecules or nanoparticles, and the extraordinarily high affinity of the interaction make the complex a superior choice for immobilization, labeling, or detection of molecules.<sup>2–5</sup>

Recombinant core streptavidin monomers consist of the residues 13–159 of wild-type streptavidin and form a stable tetramer (Figure 1A). Every streptavidin subunit consists of a  $\beta$ -barrel in which a biotin molecule can be bound. The  $\beta$ -barrel is built up from eight antiparallel  $\beta$ -strands. The four  $\beta$ -strands located toward the N-terminus are considerably shorter (5–7 amino acids) than the four  $\beta$ -strands situated toward the C-terminus (10–13 amino acids). The four long  $\beta$ -strands and the residues in between mainly mediate the interaction with the other subunits. The short  $\alpha$ -helix between seventh and eighth  $\beta$ -strand exhibits a tryptophan residue (TRP120) that reaches into a neighboring subunit and stabilizes this neighboring biotin binding pocket.<sup>6–8</sup>

The binding of biotin induces a conformational change in the molecule: The flexible loop between third and fourth  $\beta$ -strand

(L3/4; residues 45–52) closes like a lid over the binding pocket.<sup>9</sup> Crystal structures of open and closed conformation have been solved.<sup>10</sup> Loop closure is vital for the tight binding of biotin. By mutating three residues (N23A, S27D, S45A) that are important for a stable closed loop conformation (cf. Supporting Information), Howarth et al. engineered a SA subunit with negligible affinity toward biotin (Figure S3).<sup>11</sup> Interestingly, all mutated residues are located between the L3/4-loop and the N-terminus.

Combining three nonfunctional subunits with one functional subunit, defined monovalent streptavidin (mSA) enabling a 1:1 binding stoichiometry can be created. Recently, the crystal structure of mSA was solved (Figure S4).<sup>12</sup> Crystallographic data suggest that in the nonfunctional subunit, the L3/4-loop is fixed in an open state—similar to the open state of wild-type apo-SA.

Over the last decades, scientists put a lot of effort in investigating the mechanical properties of this outstanding, non-covalent interaction. It was the first receptor ligand system where binding forces between individual molecules were measured by

**Received:** October 9, 2018

**Revised:** October 18, 2018

**Published:** October 22, 2018

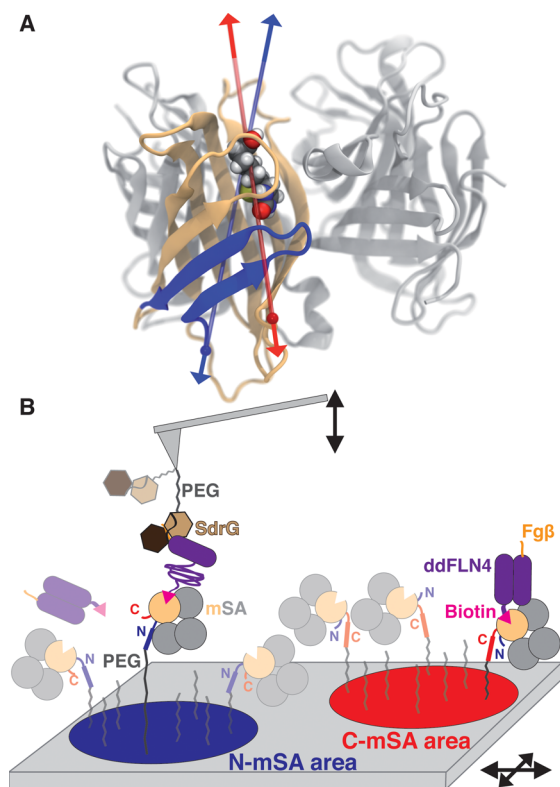


**Figure 1.** (A) Crystal structure of monovalent streptavidin (PDB 5TO2,<sup>12</sup> biotin from PDB 1MK5).<sup>43</sup> Biotin is bound in the functional subunit (light orange). The other subunits (gray) are genetically engineered to not bind biotin. Blue and red balls mark, respectively, the N- and C-terminus where mSA is tethered. Blue and red lines indicate the force loading directions. N-terminal region  $\beta$ -strands are highlighted in blue. (B) Experimental setup for AFM-based SMFS. At different surface areas, N-mSA and C-mSA are immobilized using PEG-spacers. Biotinylated (magenta) ddFLN4 (purple) is added to the solution and binds to the functional subunit of mSA (light orange ball). When the cantilever tip, functionalized with SdrG (brown hexagons), is approached to the surface, the Fg $\beta$ -peptide (orange) fused to ddFLN4 can bind to SdrG. Retracting the cantilever tip from the surface, ddFLN4 unfolds before biotin unbinds from mSA. Details of attachment chemistry and measurement process are provided in Figures S1 and S2.

atomic force microscopy (AFM)-based single molecule force spectroscopy (SMFS).<sup>13,14</sup> Unspecifically adsorbed biotinylated bovine serum albumin was immobilized on both cantilever and sample surface, while streptavidin was added to the buffer solution.<sup>15</sup> In subsequent studies, the experimental setup was improved using, for example, covalent attachment of biotin, polyethylene glycol linkers,<sup>16</sup> or other attachment strategies.<sup>17–22</sup> Later, covalent attachment of both biotin and streptavidin to cantilever or sample surface was accomplished.<sup>23,24</sup> Nowadays, the streptavidin/biotin system serves as a standard molecular anchoring system in AFM-based SMFS,<sup>25,26</sup> but also in optical tweezers,<sup>27</sup> magnetic tweezers,<sup>28</sup> and acoustic force spectroscopy experiments.<sup>29</sup>

Avidin/biotin and SA/biotin complexes were also fundamental in the initial development of steered molecular dynamics (SMD) simulations with both complexes among the first ones investigated by this technique.<sup>30,31</sup> Even before the advent of SMD, theoretical models have been put forward to describe the underlying molecular mechanism of the system.<sup>32–35</sup> Molecular dynamics (MD) simulations provided insights into different aspects of the interaction.<sup>9,36,37</sup> However, to investigate

SA/biotin mechanics, the center of mass of the SA molecule has been kept fixed in previous SMD studies, which is different from the experimental force loading geometry.<sup>30,38</sup> In the literature, a large number of experimental and theoretical results, including supposedly contradictory studies, can be found.<sup>39,40</sup> On a molecular scale, a complete understanding of how biotin unbinds from the SA binding pocket under force is to date still missing.

For this study, we produced two different variants of mSA adding a unique cysteine either on the N-terminus (N-mSA) or the C-terminus (C-mSA) of the functional subunit (Figure 1A). The cysteine is utilized for site-specific covalent tethering. Additionally, the functional subunit was equipped with a poly-histidine tag used for purification. To ensure that the modifications do not affect the binding of biotin, we performed isothermal titration calorimetry (Figure S6).

In our experiments, the two different mSA variants were immobilized a few millimeters apart from each other on a glass slide by site-specific thiol maleimide coupling to polyethylene glycol (PEG) spacers (Figure 1B). The covalent immobilization of different proteins on the same surface is advantageous, because all are probed with the same cantilever tip. This allows for direct comparison of relative forces, thus avoiding issues of cantilever calibration or measurement conditions.<sup>41,42</sup>

We used the fourth filamin domain of *Dictyostelium discoideum* (ddFLN4) as fingerprint domain to identify single-molecule interactions, because it unfolds at forces lower than biotin unbinding from mSA.<sup>44–46</sup> We performed measurements with biotinylated ddFLN4 directly covalently attached to the cantilever tip (Figures S11–13). However, the high affinity of the mSA/biotin interaction causes a rapid loss of interaction as the cantilever tip gets clogged by mSA that was nonspecifically adsorbed to the surface.

To prevent cantilever clogging and to obtain better statistics, we introduced a second receptor–ligand pair (Figure 1B). While the surface was functionalized with mSA, the cantilever was functionalized with the adhesin SD-repeat protein G (SdrG) from *Staphylococcus epidermidis*.<sup>47,48</sup> After about a thousand approach–retraction cycles, biotinylated ddFLN4, to which short peptide from human fibrinogen  $\beta$  (Fg $\beta$ ) had been genetically fused, was added to the measurement buffer. These molecules bound to the mSA on the surface via the biotin. The SdrG domain on the cantilever tip could pick up the Fg $\beta$ -peptide. Because the SdrG/Fg $\beta$  interaction can withstand a nearly 10-fold higher force than the mSA/biotin interaction,<sup>48</sup> we only measure the unbinding of biotin from mSA without bias from the SdrG/Fg $\beta$  interaction. On the other hand, the lower affinity of the SdrG/Fg $\beta$  interaction allows for a continuous exchange of the complexes at the tip and by means of this prevents permanent clogging of the cantilever tip. Even after 75 000 approach–retraction cycles, we still observed specific interactions between proteins immobilized on tip and surface (Figure 2).

The characteristic two-step unfolding pattern of ddFLN4 is used to identify single-molecule interactions, that is, a single biotin molecule binding to a single mSA molecule. In Figure 3A, two exemplary force–extension traces for single-molecule interaction on the area where N-mSA or C-mSA were immobilized are depicted (cantilever retraction velocity: 1,600 nm/s). Although the ddFLN4 unfolding is observed at the same force (Figures S7, S8), the final force peaks reach different values. These last peaks are attributed to the unbinding of biotin from mSA. Selecting all force curves that clearly show single-molecule interaction, we plotted mSA/biotin unbinding force histograms

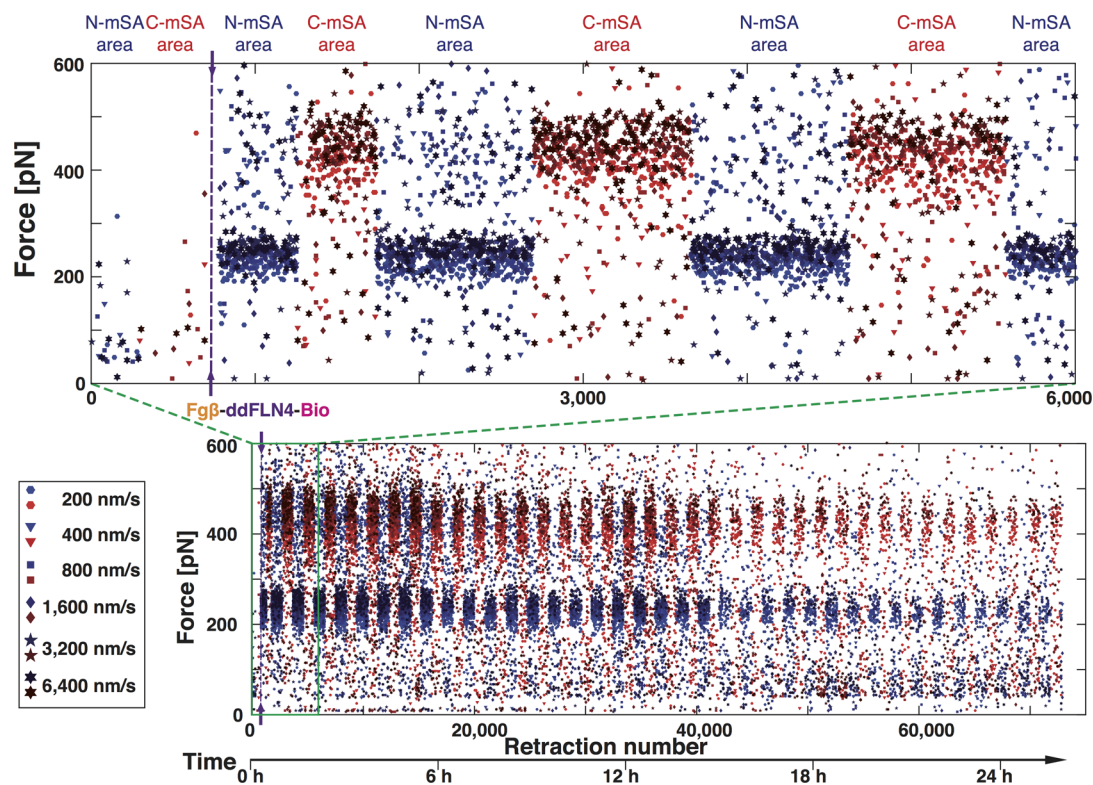


**Figure 2.** Course of a measurement. The final unbinding forces for all retractions of the cantilever tip from the surface are shown. Interactions on the surface area with the C-mSA are plotted in red colors; interactions in the N-mSA area are shown in blue colors. The darker the color is, the higher the cantilever retraction velocity is. The beginning of the measurement is shown on top. The  $\text{Fg}\beta$ -ddFLN4-Biotin construct was added after 960 approaches, indicated by the purple dashed line and arrows. At the beginning of the measurement, high unbinding forces for N-mSA are also observed which are attributed to multiple interactions.

for both attachment geometries and all six retraction velocities (Figure 3B). We used Bell-Evans theory to fit the peaks of the distributions (Tables S1, S2).<sup>49,50</sup> While biotin unbinds from N-terminally tethered mSA at forces of about 200 pN, its binding to C-terminally tethered mSA is mechanically more stable and withstands forces of more than 400 pN. Fitting the dynamic force spectrum (Figure 3C), we could draw conclusions about coarse features of the binding energy landscape: by a factor of 2, the potential well is narrower for C-mSA compared to N-mSA.

To reveal the underlying molecular mechanism of the mSA/ biotin interaction, ensuring statistical reliability, we performed 150 SMD production runs, which combined account for 19  $\mu\text{s}$ . Simulations were performed using QwikMD<sup>51</sup> and GPU-accelerated NAMD.<sup>52,53</sup> In previous SMD studies, usually the center of mass of the SA molecules was kept at a fixed position, which does not resemble the experimental conditions. In our SMD simulations, we hold mSA either by the C-terminus or the N-terminus of the functional subunit and pulled biotin out of the binding pocket (for details on the preparation of the system, cf. Supporting Information), which is in agreement with the experimentally applied force loading geometry (Figure 1A). While for C-mSA, a unimodal force distribution was observed (Figure 4A), N-mSA showed a bimodal behavior (Figure 4B,C). For 9 out of 25 SMD replicas performed at 5000  $\mu\text{m}/\text{s}$  pulling speed, the structural integrity of the N-terminal  $\beta$ -sheet was destroyed, before biotin left the binding pocket (Figure 4E). This structural rearrangement weakens the stability of the N-terminal  $\beta$ -sheet structure and thus results in lower final unbinding forces, blurring the boundaries between unbinding and unfolding. In one case, due to an extended simulation time

we even observed how streptavidin regains its native fold when the force drops after biotin has left the pocket. The number of H-bonds between the first and the second  $\beta$ -strand provides a measure for the structural integrity (Figure 4G). If the N-terminal  $\beta$ -sheet structure stays intact, the number of H-bonds stays constant over time and high unbinding forces can be reached. The small unfolding observed in the simulations is beyond the resolution of our experimental setup. As the force loading rate dependence of an unfolding or unbinding event can be completely different than the one of a direct unbinding event, the simulations can be favoring the latter type of event while the experiments the former.

The simulations provide a detailed picture of the unbinding process, with atomic spatial resolution and femtosecond time resolution. Using correlation-based network analysis (Figures S14–16),<sup>54</sup> we analyzed the force propagation profiles, identifying which amino acids and domains of the molecules transmit force.<sup>55</sup> For C-mSA (Figure 5A–C), force either propagates through the long C-terminal  $\beta$ -strand, or through the N-terminal  $\beta$ -sheet structure, near the first hairpin between  $\beta$ -strands 1 and 2. These pathways indicate that mSA is structurally stable from both biotin sides when force is applied at the C-terminus, comparable with a claw. For N-mSA (Figure 5D–F), on the other hand, force is only rarely transmitted through the long C-terminal  $\beta$ -strands. Force propagates mainly through the shorter N-terminal  $\beta$ -strands. As the tension is high over the first and the second  $\beta$ -strand, high rupture forces can be reached if this region stays intact (Figure 5F). If the first two  $\beta$ -strands get torn apart (Figure 5E), the N-terminal structure loosens, mSA releases its grip on biotin, and biotin leaves the binding pocket.

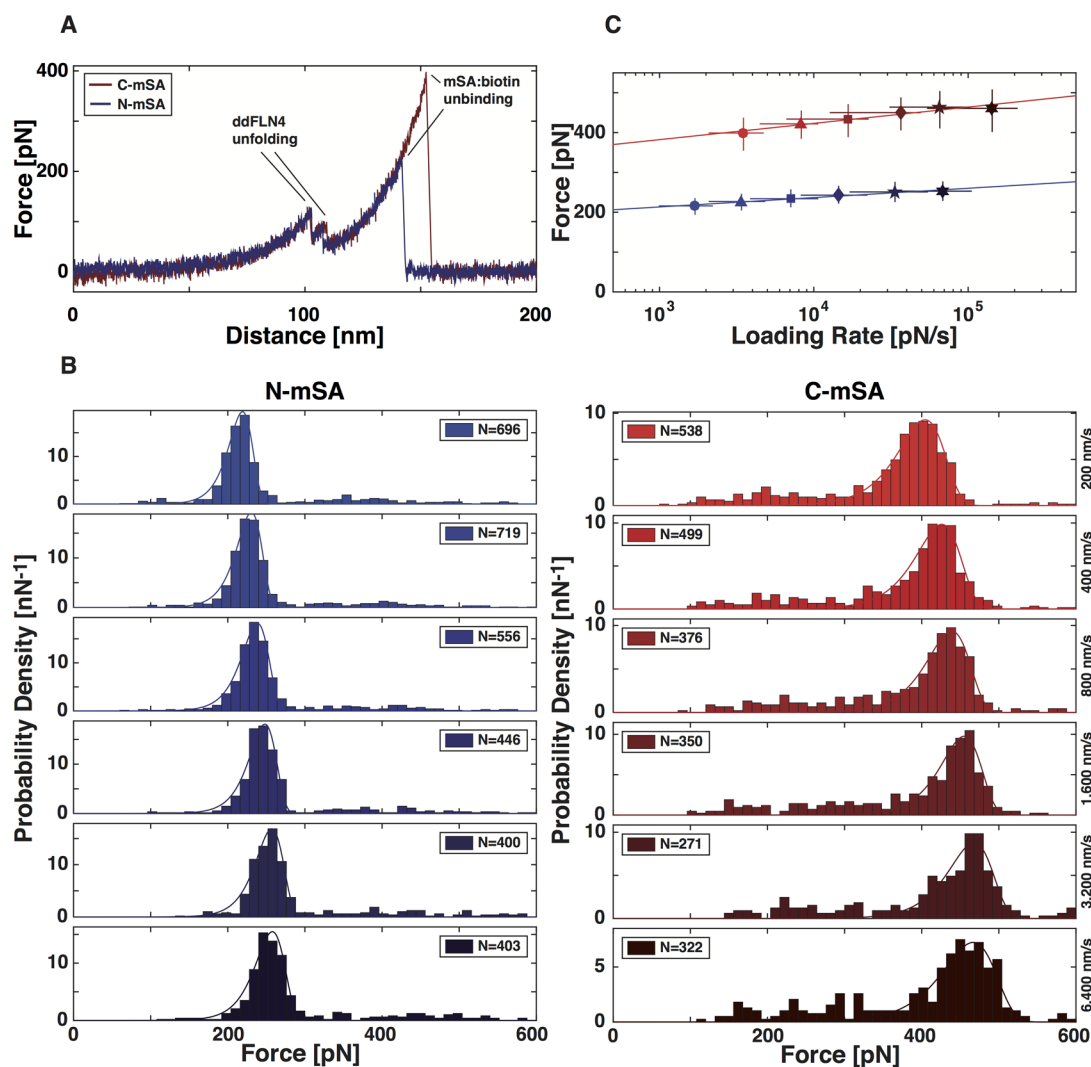


**Figure 3.** Analysis of force curves showing characteristic unfolding pattern. (A) Exemplary force extension traces measured at a retraction velocity of 1600 nm/s for C-mSA (red) and N-mSA (blue) displaying the characteristic two peak unfolding pattern of ddFLN4. Only traces showing this pattern are selected for further analysis. (B) Force histograms of mSA/biotin unbinding for six different retraction velocities. Peaks are fitted with Bell-Evans distributions (solid lines). (C) For all retraction velocities, the most probable unbinding force is plotted against the most probable loading rate and fitted according to Bell-Evans theory. From the fit, distance to transition state  $\Delta x_0$  and zero-force off-rate  $k_{\text{off},0}$  are determined. N-mSA:  $\Delta x_0 = 0.41$  nm,  $k_{\text{off},0} = 7.7 \times 10^{-8} \text{ s}^{-1}$ ; C-mSA:  $\Delta x_0 = 0.23$  nm,  $k_{\text{off},0} = 2.5 \times 10^{-8} \text{ s}^{-1}$ . Error bars are given by the full width at half-maximum of the peak of the corresponding distribution.

When there is no more tension on the mSA subunit, the native N-terminal structure is retrieved. The importance of the N-terminal structural integrity is in line with the fact that all mutations needed to generate the nonfunctional subunit, are at prominent positions within the N-terminal  $\beta$ -sheet structure (cf. Supporting Information).

SMD trajectories were also employed to investigate the contact between biotin and SA. Using PyContact,<sup>56</sup> we created a map of the interactions between ligand and receptor. Initially, the contact score was analyzed throughout the whole simulation time for each of the trajectories. To better understand the differences in an equilibrium versus a force-loaded regime, we compared the contact score over trajectory windows under no force load and under high-force load. The analysis was performed for all 50 slow pulling trajectories performed at 5000  $\mu\text{m/s}$  pulling speed (25 for N-terminal pulling and 25 for C-terminal pulling). Additionally, the root-mean-square fluctuation (RMSF) was also analyzed in the same trajectory windows. Because of the large amount of data generated in such analysis,

a “big-data” strategy of dimensionality reduction had to be adopted. The analysis was performed using python libraries through Jupyter Notebook.<sup>57</sup> Commonly known as machine learning techniques, our approach employed mutual information theory to identify the amino acid residues that were “force-active”. These residues were coupled to changes in force and could indicate possible key points of force regulation. Indeed, most of these residues had been previously identified as key-players in the mechanism of SA/biotin interaction (Tables S3 and S4).

Combined, the analysis of the SMD trajectories indicate that the partial unfolding for N-terminal force loading is the cause of the lower forces seen for N-mSA compared with C-mSA in the experiments. The second N-terminal pulling unbinding pathway seen in the simulations is only rarely observed in the experiments, as indicated by the small number of high-force events in Figure 3B. On the one hand, this might be due to the much faster pulling speeds of the simulations. In the experiment, the force loading rates are at least four orders of magnitude

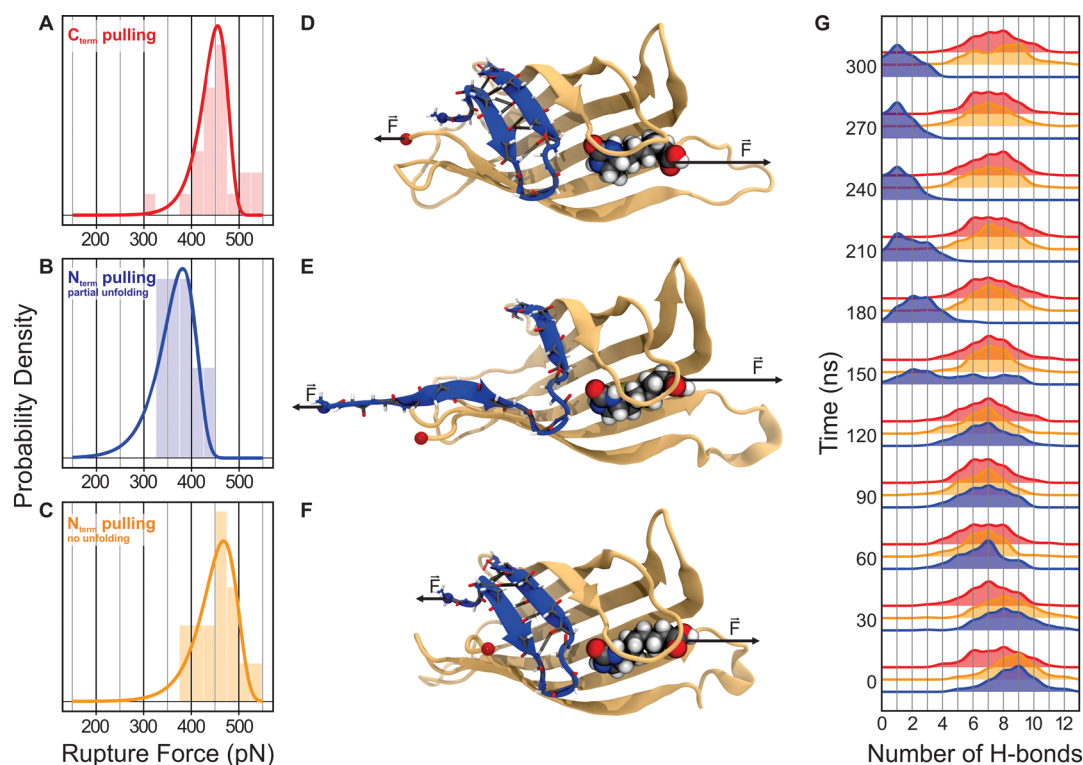


**Figure 4.** Results of SMD simulations. Unbinding force histogram for C-terminal attachment of mSA shows a unimodal distribution (red, A) ( $N = 25$ ). For N-terminal attachment of mSA, two unbinding force peaks are observed: One at lower forces (blue, B) ( $N = 9$ ) and one at higher forces (yellow, C) ( $N = 16$ ). For C-terminal attachment of mSA, the structural integrity of the N-terminal  $\beta$ -sheet (marked in blue) is preserved (D). For N-terminal attachment of mSA, the structure of the N-terminal  $\beta$ -sheet can be destroyed before biotin unbinds from mSA, resulting in lower unbinding forces (E). If it stays intact, higher unbinding forces are reached (F). The number of hydrogen bonds between the first and the second N-terminal  $\beta$ -strand is a good measure to differentiate both cases (G). For the C-terminal attachment of mSA, it stays roughly constant over the timespan of the simulation (red). For N-terminal attachment, the contact is either broken completely (blue) or only slightly attenuated (yellow).

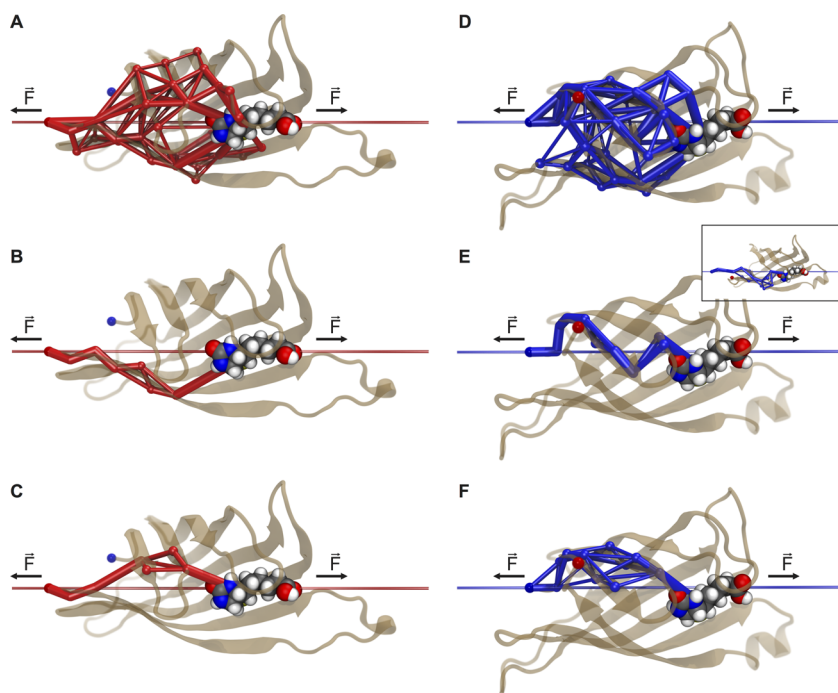


**Figure 5.** Force propagation pathways through the functional mSA subunit. (A) Overlay of the force propagation pathways for simulation replicas with C-terminal loading (Video S2) ( $N = 25$ ). Force propagates through C-terminal  $\beta$ -sheets (B) or also through N-terminal  $\beta$ -sheets (C). (D) Overlay of all force propagation pathways for all simulation replicas with N-terminal loading (Video S3) ( $N = 25$ ). Force propagates through N-terminal  $\beta$ -sheets. If the structural integrity of the N-terminal  $\beta$ -sheets is destroyed, the unbinding forces are low (E). If the N-terminal structure stays intact, higher unbinding forces can be reached (F). The thickness of the pathway edges represents the probability of force propagating through the particular edge. The probability was normalized for each simulation, leading to the same maximum thickness (maximum information pathway) for each simulation replica.

lower. The N-terminal  $\beta$ -sheet structure is held under tension for a much longer time, such that the unzipping of the first from the second  $\beta$ -strand is more likely. On the other hand, the molecular linker of the biotin to Coenzyme A (for details of the biotinylation, cf. Supporting Information) is not considered in the simulations (Figure S5) because there is no crystal structure for the linker and in addition missing force field parameters could introduce a source of imprecision. In previous combined AFM SMD studies, it was shown that only a complete simulation of all molecular linkers in proximity of the protein of interest provided an excellent agreement between experimental and simulated forces.<sup>48</sup> It is yet reasonable to assume that the additional interaction of the linker between biotin and Coenzyme A with mSA increases the final unbinding forces of biotin from mSA. Such interaction would favor the N-mSA unzipping/low force unbinding pathway over the high force unbinding pathway even more, also explaining the different in force distribution between simulation and experiment.

In this study, experiments and simulations were used hand-in-hand, providing a detailed picture of the system mechanics with the atomistic detail of the simulation, substantiated by the large statistical content of experiments. The nearly twofold difference in unbinding forces that we report for biotin in the two well-defined N- and C-terminal tethering geometries of mSA is nicely matched by the 2-fold reduction of the binding potential width as revealed by the Bell-Evans analysis of the rate dependence of the unbinding forces. Because we measured by ITC the same binding energy for the mSA/biotin complexes in both tethering geometries, we can conclude that our force histograms represent largely homogeneous ensembles of unbinding modes. The analysis of these modes by steered SMD revealed that in the case of the C-terminally tethered mSA the forced separation of biotin can be described best by a rupture process, leaving the molecular structure of the mSA binding pocket largely intact. The N-terminally tethered mSA, however, shows in a significant number of traces a marked structural change, a local unfolding of the binding pocket. We assume that the much slower time scale of the AFM-based SMFS favors the low force unfolding path. This partial unfolding results in a substantial widening of the potential energy landscape accompanied by a reduction of the unbinding force for N-mSA compared to C-mSA. In view on our results, it is worth noting that the widespread of SA/biotin unbinding forces reported in the literature<sup>39,40</sup> may have arisen from a multiplicity of force propagation geometries due to the nonspecific immobilization of the tetrameric streptavidins used in these investigations.

## ■ ASSOCIATED CONTENT

### 📄 Supporting Information

The Supporting Information is available free of charge on the ACS Publications website at DOI: 10.1021/acs.nanolett.8b04045.

Materials and methods, results of isothermal titration calorimetry, results of SMFS with covalent attachment of ddFLN4, fit parameter of Bell-Evans fits, results of mutual information analysis, protein sequences (PDF)

Steered molecular dynamics simulations. Analyses of C- versus N-terminal pulling reveal that the instability of N-terminal region during the latter pulling is fundamental for the differences observed in force traces (AVI)

Exposé of all force propagation pathways for all simulation replicas with C-terminal loading (AVI)

Exposé of all force propagation pathways for all simulation replicas with N-terminal loading (AVI)

## ■ AUTHOR INFORMATION

### Corresponding Author

\*E-mail: rcbernardi@ks.uiuc.edu.

### ORCID

Steffen M. Sedlak: 0000-0002-7037-1793

Leonard C. Schendel: 0000-0002-1986-2693

Marcelo C. R. Melo: 0000-0001-6901-1646

Hermann E. Gaub: 0000-0002-4220-6088

Rafael C. Bernardi: 0000-0003-0758-2026

### Author Contributions

The manuscript was written through contributions of all authors. All authors have given approval to the final version of the manuscript.

### Author Contributions

<sup>†</sup>S.M.S. and L.C.S. contributed equally.

### Funding

The European Research Council (ERC advanced grant Cellufuel Grant 294438) and the Deutsche Forschungsgemeinschaft (DFG, Sonderforschungsbereich 1032, Teilprojekt A01) provided funding for this work. Furthermore, it was supported by the National Institutes of Health (NIH) Grant P41-GM104601, "Center for Macromolecular Modeling and Bioinformatics". R.C.B. is partially supported by National Science Foundation (NSF) Grant MCB-1616590, "Molecular Modeling of Bioenergetic Systems". Molecular dynamics simulations made use of GPU-accelerated nodes of Blue Waters supercomputer as part of the Petascale Computational Resource (PRAC) grant "The Computational Microscope", which is supported by the National Science Foundation (award number ACI-1713784). The state of Illinois and the National Science Foundation (awards OCI-0725070 and ACI-1238993) support Blue Waters sustained-petascale computing project.

### Notes

The authors declare no competing financial interest.

## ■ ACKNOWLEDGMENTS

The authors thank A. Kardinal and T. Nicolaus for laboratory support, L.F. Milles for providing the SdrG/Fg $\beta$ -system, and M. Scheurer for assistance with integrating PyContact and Jupyter. The authors acknowledge M.S. Bauer and C. Kluger for helpful discussions. S.M.S. thanks the Nanosystems Initiative Munich for support.

## ■ ABBREVIATIONS

SA, streptavidin; AFM, atomic force microscopy; SMFS, single-molecule force spectroscopy; SMD, steered molecular dynamics; mSA, monovalent streptavidin; N-mSA, N-terminally tethered monovalent streptavidin; C-mSA, C-terminally tethered monovalent streptavidin; ddFLN4, fourth filamin domain of *Dictyostelium discoideum*; SdrG, SD-repeat protein G from *Staphylococcus epidermidis*; Fg $\beta$ , a short peptide from human fibrinogen  $\beta$

## ■ REFERENCES

- (1) Dundas, C. M.; Demonte, D.; Park, S. *Appl. Microbiol. Biotechnol.* **2013**, *97* (21), 9343–53.
- (2) Wilchek, M.; Bayer, E. A. *Anal. Biochem.* **1988**, *171* (1), 1–32.
- (3) Bayer, E. A.; Ben-Hur, H.; Wilchek, M. *Methods Enzymol.* **1990**, *184*, 80–9.
- (4) Green, N. M. *Methods Enzymol* **1990**, *184*, 51–67.

- (5) Laitinen, O. H.; Nordlund, H. R.; Hytonen, V. P.; Kulomaa, M. S. *Trends Biotechnol.* **2007**, *25* (6), 269–77.
- (6) Freitag, S.; Le Trong, I.; Chilkoti, A.; Klumb, L. A.; Stayton, P. S.; Stenkamp, R. E. *J. Mol. Biol.* **1998**, *279* (1), 211–21.
- (7) Lim, K. H.; Huang, H.; Pralle, A.; Park, S. *Biotechnol. Bioeng.* **2013**, *110* (1), 57–67.
- (8) Scholl, Z. N.; Yang, W.; Marszalek, P. E. *ACS Nano* **2015**, *9* (2), 1189–97.
- (9) Bansal, N.; Zheng, Z.; Song, L. F.; Pei, J.; Merz, K. M., Jr. *J. Am. Chem. Soc.* **2018**, *140* (16), 5434–5446.
- (10) Freitag, S.; Le Trong, I.; Klumb, L.; Stayton, P. S.; Stenkamp, R. E. *Protein Sci.* **1997**, *6* (6), 1157–1166.
- (11) Howarth, M.; Chinnapen, D. J.; Gerrow, K.; Dorrestein, P. C.; Grandy, M. R.; Kelleher, N. L.; El-Husseini, A.; Ting, A. Y. *Nat. Methods* **2006**, *3* (4), 267–73.
- (12) Zhang, M.; Biswas, S.; Deng, W.; Yu, H. *Sci. Rep.* **2016**, *6*, 35915.
- (13) Florin, E. L.; Moy, V. T.; Gaub, H. E. *Science* **1994**, *264* (5157), 415–7.
- (14) Lee, G.; Kidwell, D.; Colton, R. *Langmuir* **1994**, *10* (2), 354–357.
- (15) Moy, V. T.; Florin, E. L.; Gaub, H. E. *Science* **1994**, *266* (5183), 257–9.
- (16) Merkel, R.; Nassoy, P.; Leung, A.; Ritchie, K.; Evans, E. *Nature* **1999**, *397* (6714), 50–3.
- (17) Wong, J.; Chilkoti, A.; Moy, V. T. *Biomol. Eng.* **1999**, *16* (1–4), 45–55.
- (18) Stevens, M. M.; Allen, S.; Davies, M. C.; Roberts, C. J.; Schacht, E.; Tendler, S. J. B.; VanSteenkiste, S.; Williams, P. M. *Langmuir* **2002**, *18* (17), 6659–6665.
- (19) Yuan, C.; Chen, A.; Kolb, P.; Moy, V. T. *Biochemistry* **2000**, *39* (33), 10219–23.
- (20) Lo, Y.-S.; Zhu, Y.-J.; Beebe, T. P. *Langmuir* **2001**, *17* (12), 3741–3748.
- (21) Rico, F.; Moy, V. T. *J. Mol. Recognit.* **2007**, *20* (6), 495–501.
- (22) de Odrowaz Piramowicz, M.; Czuba, P.; Targosz, M.; Burda, K.; Szymanski, M. *Acta Biochim Pol* **2006**, *53* (1), 93–100.
- (23) Taninaka, A.; Takeuchi, O.; Shigekawa, H. *Int. J. Mol. Sci.* **2010**, *11* (5), 2134–51.
- (24) Sedlak, S. M.; Bauer, M. S.; Kluger, C.; Schendel, L. C.; Milles, L. F.; Pippig, D. A.; Gaub, H. E. *PLoS One* **2017**, *12* (12), e0188722.
- (25) Ott, W.; Jobst, M. A.; Schoeler, C.; Gaub, H. E.; Nash, M. A. *J. Struct. Biol.* **2017**, *197* (1), 3–12.
- (26) Walder, R.; LeBlanc, M. A.; Van Patten, W. J.; Edwards, D. T.; Greenberg, J. A.; Adhikari, A.; Okoniewski, S. R.; Sullan, R. M. A.; Rabuka, D.; Sousa, M. C.; Perkins, T. T. *J. Am. Chem. Soc.* **2017**, *139* (29), 9867–9875.
- (27) Tych, K. M.; Jahn, M.; Gegenfurtner, F.; Hecht, V. K.; Buchner, J.; Hugel, T.; Rief, M. *J. Phys. Chem. B* **2018**.
- (28) Kriegel, F.; Ermann, N.; Forbes, R.; Dulin, D.; Dekker, N. H.; Lipfert, J. *Nucleic Acids Res.* **2017**, *45*, 5920.
- (29) Sitters, G.; Kamsma, D.; Thalhammer, G.; Ritsch-Marte, M.; Peterman, E. J.; Wuite, G. J. *Nat. Methods* **2015**, *12* (1), 47–50.
- (30) Grubmuller, H.; Heymann, B.; Tavan, P. *Science* **1996**, *271* (5251), 997–9.
- (31) Izrailev, S.; Stepaniants, S.; Balsera, M.; Oono, Y.; Schulten, K. *Biophys. J.* **1997**, *72* (4), 1568–81.
- (32) Chilkoti, A.; Stayton, P. S. *J. Am. Chem. Soc.* **1995**, *117* (43), 10622–10628.
- (33) Chilkoti, A.; Boland, T.; Ratner, B. D.; Stayton, P. S. *Biophys. J.* **1995**, *69* (5), 2125–30.
- (34) Pincet, F.; Husson, J. *Biophys. J.* **2005**, *89* (6), 4374–81.
- (35) Guo, S.; Ray, C.; Kirkpatrick, A.; Lad, N.; Akhremitchev, B. B. *Biophys. J.* **2008**, *95* (8), 3964–3976.
- (36) Song, J.; Li, Y.; Ji, C.; Zhang, J. Z. H. *Sci. Rep.* **2015**, *5*, 7906.
- (37) Liu, F.; Zhang, J. Z. H.; Mei, Y. *Sci. Rep.* **2016**, *6*, 27190.
- (38) Rico, F.; Russek, A.; Gonzalez, L.; Grubmuller, H.; Scheuring, S. **2018** arXiv preprint arXiv:1808.07122.
- (39) Zlatanova, J.; Lindsay, S. M.; Leuba, S. H. *Prog. Biophys. Mol. Biol.* **2000**, *74* (1–2), 37–61.
- (40) Teulon, J. M.; Delcuze, Y.; Odorico, M.; Chen, S. W.; Parot, P.; Pellequer, J. L. *J. Mol. Recognit.* **2011**, *24* (3), 490–502.
- (41) Verdorfer, T.; Bernardi, R. C.; Meinhold, A.; Ott, W.; Luthy-Schulten, Z.; Nash, M. A.; Gaub, H. E. *J. Am. Chem. Soc.* **2017**, *139* (49), 17841–17852.
- (42) Verdorfer, T.; Gaub, H. E. *Sci. Rep.* **2018**, *8* (1), 9634.
- (43) Hyre, D. E.; Le Trong, I.; Merritt, E. A.; Eccleston, J. F.; Green, N. M.; Stenkamp, R. E.; Stayton, P. S. *Protein Sci.* **2006**, *15* (3), 459–67.
- (44) Schwaiger, I.; Kardinal, A.; Schleicher, M.; Noegel, A. A.; Rief, M. *Nat. Struct. Mol. Biol.* **2004**, *11* (1), 81–5.
- (45) Milles, L. F.; Bayer, E. A.; Nash, M. A.; Gaub, H. E. *J. Phys. Chem. B* **2017**, *121* (15), 3620–3625.
- (46) Bauer, M. S.; Milles, L. F.; Sedlak, S. M.; Gaub, H. E. **2018**, *bioRxiv*.
- (47) Herman, P.; El-Kirat-Chatel, S.; Beaussart, A.; Geoghegan, J. A.; Foster, T. J.; Dufrene, Y. F. *Mol. Microbiol.* **2014**, *93* (2), 356–68.
- (48) Milles, L. F.; Schulten, K.; Gaub, H. E.; Bernardi, R. C. *Science* **2018**, *359* (6383), 1527–1533.
- (49) Bell, G. I. *Science* **1978**, *200* (4342), 618–27.
- (50) Evans, E.; Ritchie, K. *Biophys. J.* **1997**, *72* (4), 1541–55.
- (51) Ribeiro, J. V.; Bernardi, R. C.; Rudack, T.; Stone, J. E.; Phillips, J. C.; Freddolino, P. L.; Schulten, K. *Sci. Rep.* **2016**, *6*, 26536.
- (52) Phillips, J. C.; Braun, R.; Wang, W.; Gumbart, J.; Tajkhorshid, E.; Villa, E.; Chipot, C.; Skeel, R. D.; Kale, L.; Schulten, K. *J. Comput. Chem.* **2005**, *26* (16), 1781–802.
- (53) Melo, M. C. R.; Bernardi, R. C.; Rudack, T.; Scheurer, M.; Riplinger, C.; Phillips, J. C.; Maia, J. D. C.; Rocha, G. B.; Ribeiro, J. V.; Stone, J. E.; Neese, F.; Schulten, K.; Luthy-Schulten, Z. *Nat. Methods* **2018**, *15* (5), 351–354.
- (54) Sethi, A.; Eargle, J.; Black, A. A.; Luthy-Schulten, Z. *Proc. Natl. Acad. Sci. U. S. A.* **2009**, *106* (16), 6620–5.
- (55) Schoeler, C.; Bernardi, R. C.; Malinowska, K. H.; Durner, E.; Ott, W.; Bayer, E. A.; Schulten, K.; Nash, M. A.; Gaub, H. E. *Nano Lett.* **2015**, *15* (11), 7370–6.
- (56) Scheurer, M.; Rodenkirch, P.; Siggel, M.; Bernardi, R. C.; Schulten, K.; Tajkhorshid, E.; Rudack, T. *Biophys. J.* **2018**, *114* (3), 577–583.
- (57) Kluyver, T.; Benjamin, R.-K.; Fernando, P.; Brian, G.; Matthias, B.; Jonathan, F.; Kyle, K.; Jessica, H.; Jason, G.; Sylvain, C.; Paul, I.; Damián, A.; Safia, A.; Carol, W.; Jupyter Development, T. In *Jupyter Notebooks—a publishing format for reproducible computational workflows*; Positioning and Power in Academic Publishing: Players, Agents and Agendas, 20th International Conference on Electronic Publishing, Göttingen, Germany, 2016.